



Restoring Prohealing/Remodeling-Associated M2a/c Macrophages Using ON101 Accelerates Diabetic Wound Healing

Ching-Wen Lin¹, Chih-Chiang Chen^{2,3}, Wen-Yen Huang⁴, Yen-Yu Chen¹, Shiou-Ting Chen⁴, Hung-Wen Chou¹, Chien-Ming Hung⁴, Wan-Jiun Chen¹, Chia-Sing Lu⁵, Shi-Xin Nian², Shyi-Gen Chen^{1,6}, Hsuen-Wen Chang⁷, Vincent H.S. Chang^{7,8,9}, Li-Ying Liu², Ming-Liang Kuo¹⁰ and Shun-Cheng Chang¹¹

Diabetic wounds exhibit chronic inflammation and delayed tissue proliferation or remodeling, mainly owing to prolonged proinflammatory (M1) macrophage activity and defects in transition to prohealing/proremodeling (M2a/M2c; CD206⁺ and/or CD163⁺) macrophages. We found that topical treatment with ON101, a plant-based potential therapeutic for diabetic foot ulcers, increased M2c-like (CD163⁺ and CD206⁺) cells and suppressed M1-like cells, altering the inflammatory gene profile in a diabetic mouse model compared with that in the controls. An in vitro macrophage-polarizing model revealed that ON101 directly suppressed CD80⁺ and CD86⁺ M1-macrophage polarization and M1-associated proinflammatory cytokines at both protein and transcriptional levels. Notably, conditioned medium collected from ON101-treated M1 macrophages reversed the M1-conditioned medium-mediated suppression of CD206⁺ macrophages. Furthermore, conditioned medium from ON101-treated adipocyte progenitor cells significantly promoted CD206⁺ and CD163⁺ macrophages but strongly inhibited M1-like cells. ON101 treatment also stimulated the expression of *GCSF* and *CXCL3* genes in human adipocyte progenitor cells. Interestingly, treatment with recombinant GCSF protein enhanced both CD206⁺ and CD163⁺ M2 markers, whereas CXCL3 treatment only stimulated CD163⁺ M2 macrophages. Depletion of cutaneous M2 macrophages inhibited ON101-induced diabetic wound healing. Thus, ON101 directly suppressed M1 macrophages and facilitated the GCSF- and CXCL3-mediated transition from M1 to M2 macrophages, lowering inflammation and leading to faster diabetic wound healing.

JID Innovations (2022);2:100138 doi:10.1016/j.xjidi.2022.100138

¹Oneness Biotech Co., Ltd., Taipei, Taiwan; ²Department of Dermatology, Taipei Veterans General Hospital, Taipei, Taiwan; ³Department of Dermatology, School of Medicine, National Yang Ming Chiao Tung University, Taipei, Taiwan; ⁴Microbio Co., Ltd, Taipei, Taiwan; ⁵NTU YongLin Institute of Health, National Taiwan University, Taipei, Taiwan; ⁶Division of Plastic and Reconstructive Surgery, Department of Surgery, Tri-Service General Hospital, National Defense Medical Center, Taipei, Taiwan; ⁷TMU Laboratory Animal Center, Office of Research and Development, Taipei Medical University, Taipei, Taiwan; ⁸Department of Physiology, School of Medicine, Taipei Medical University, Taipei, Taiwan; ⁹The PhD Program for Translational Medicine, College of Medical Science and Technology, Taipei Medical University, Taipei, Taiwan; ¹⁰Microbio Shanghai Co., Ltd., Shanghai, China; and ¹¹Division of Plastic Surgery, Integrated Burn & Wound Care Center, Department of Surgery, Shuang-Ho Hospital; Department of Surgery, School of Medicine, College of Medicine, Taipei Medical University, Taipei, Taiwan

Correspondence: Shun-Cheng Chang, Division of Plastic Surgery, Integrated Burn & Wound Care Center, Department of Surgery, Shuang-Ho Hospital; Department of Surgery, School of Medicine, College of Medicine, Taipei Medical University, Taipei, Taiwan; Number 291, Zhongzheng Road, Zhonghe District, New Taipei City 235, Taiwan. E-mail: csc901515@gmail.com

Abbreviations: ADPC, adipocyte progenitor cell; CM, conditioned medium; HFD, high-fat diet; HG, high-glucose; IHC, immunohistochemistry; iNOS, inducible nitric oxide synthase; M1-CM, M1-associated conditioned medium; m-Clo, mannoseylated clodronate; STAT3, signal transducer and activator of transcription 3

Received 5 December 2021; revised 26 April 2022; accepted 27 April 2022; accepted manuscript published online XXX; corrected proof published online XXX

Cite this article as: *JID Innovations* 2022;2:100138

INTRODUCTION

Functional changes in macrophage subtypes from a proinflammatory (M1-like) phenotype to an anti-inflammatory/proremodeling (M2-like) phenotype are critical for the transition from inflammation to regeneration in wound healing (Gordon, 2003; Graney et al., 2020). M2 macrophages are either converted from M1 macrophages or from newly arriving monocytes with mixed phenotypes, primarily M2a, M2b, M2c, and M2d subtypes, characterized by distinctive surface markers and functions (Graney et al., 2020). M2a and M2c subtypes, obtained from M2 macrophages activated by exposure to different stimulators, are functionally characterized as prohealing and proremodeling, respectively, and are distinguished by their corresponding expression of the surface markers CD206 and CD206/CD163 (Abdelaziz et al., 2020; Graney et al., 2020).

Diabetic foot ulcers are a type of chronic wound in which hyperglycemic conditions impede the healing process. In patients with diabetes with such wounds, there is a prolonged inflammation phase featuring sustained levels of M1-like macrophages and a shortage of M2-like macrophages (quantified as a higher M1/M2 ratio) (Ganesh and Ramkumar, 2020; Huang et al., 2019; Krzyszczyk et al., 2018). In particular, sustained secretion of IL-6, TNF- α , and IL-1 family

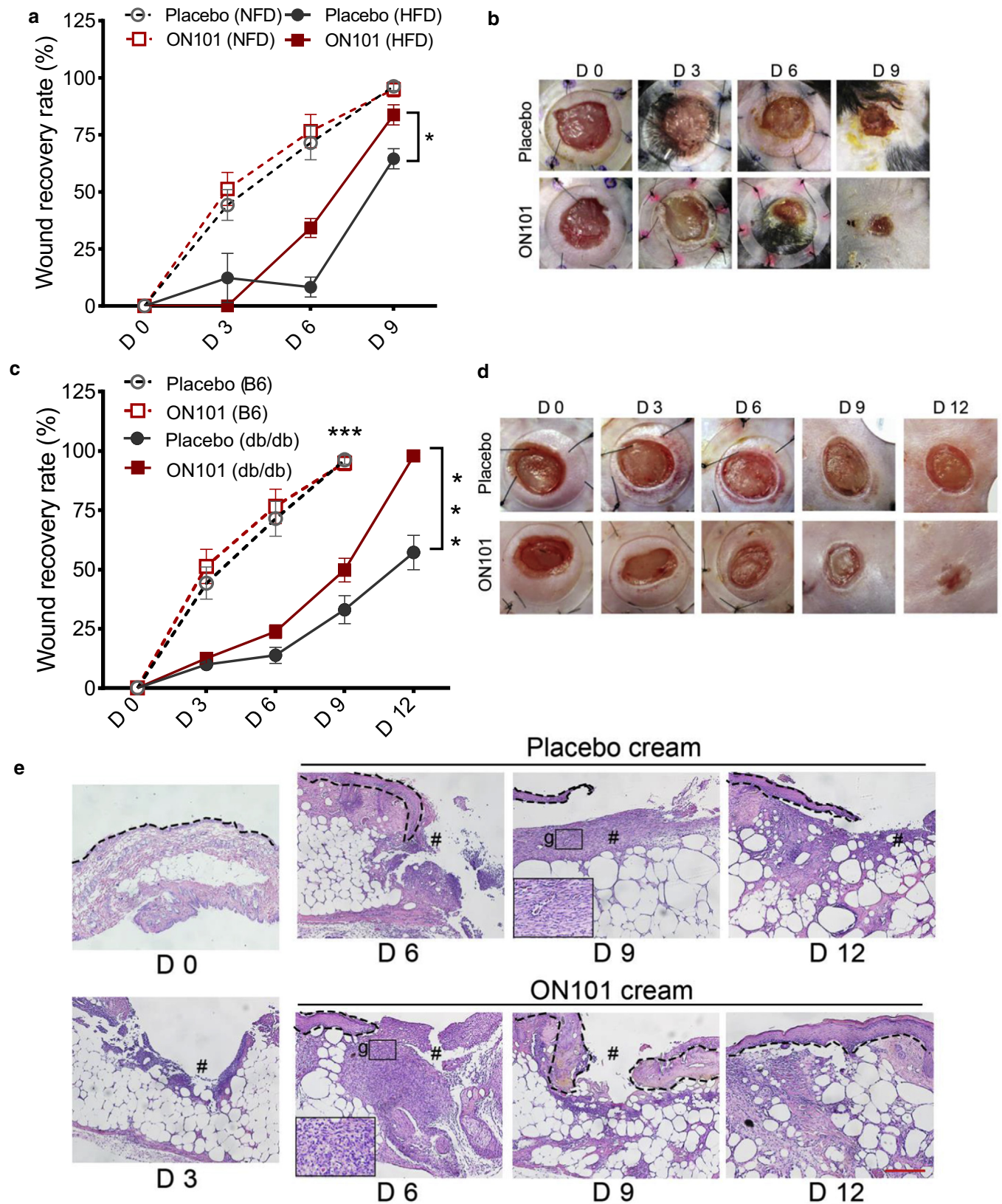


Figure 1. ON101 promotes diabetic and HFD-induced wound healing. Kinetic analysis of skin excisional wound healing (a, b) in the NFD-C57BL/6 (NFD/B6) mice and HFD-induced obesity mouse model and (c-g) in db/db mice. (a, c) Wound recovery rate measured at indicated time points given as a percentage of the change in area from D 0. Black arrows indicate the initiation of drug application (D 0 in HFD-C57BL/6 mice, D 3 in db/db mice). * $P < 0.05$ and ** $P < 0.01$ analyzed by two-way repeated-measures ANOVA; $n = 6$ in HFD group and $n = 12$ in db/db mice. H&E staining represents (e) epithelization (dotted line) and (g) granulation tissue in the indicated treatment groups; # indicates wound bed. Bar = 250 μm . D, day; HFD, high-fat diet; NFD, normal-fat diet.

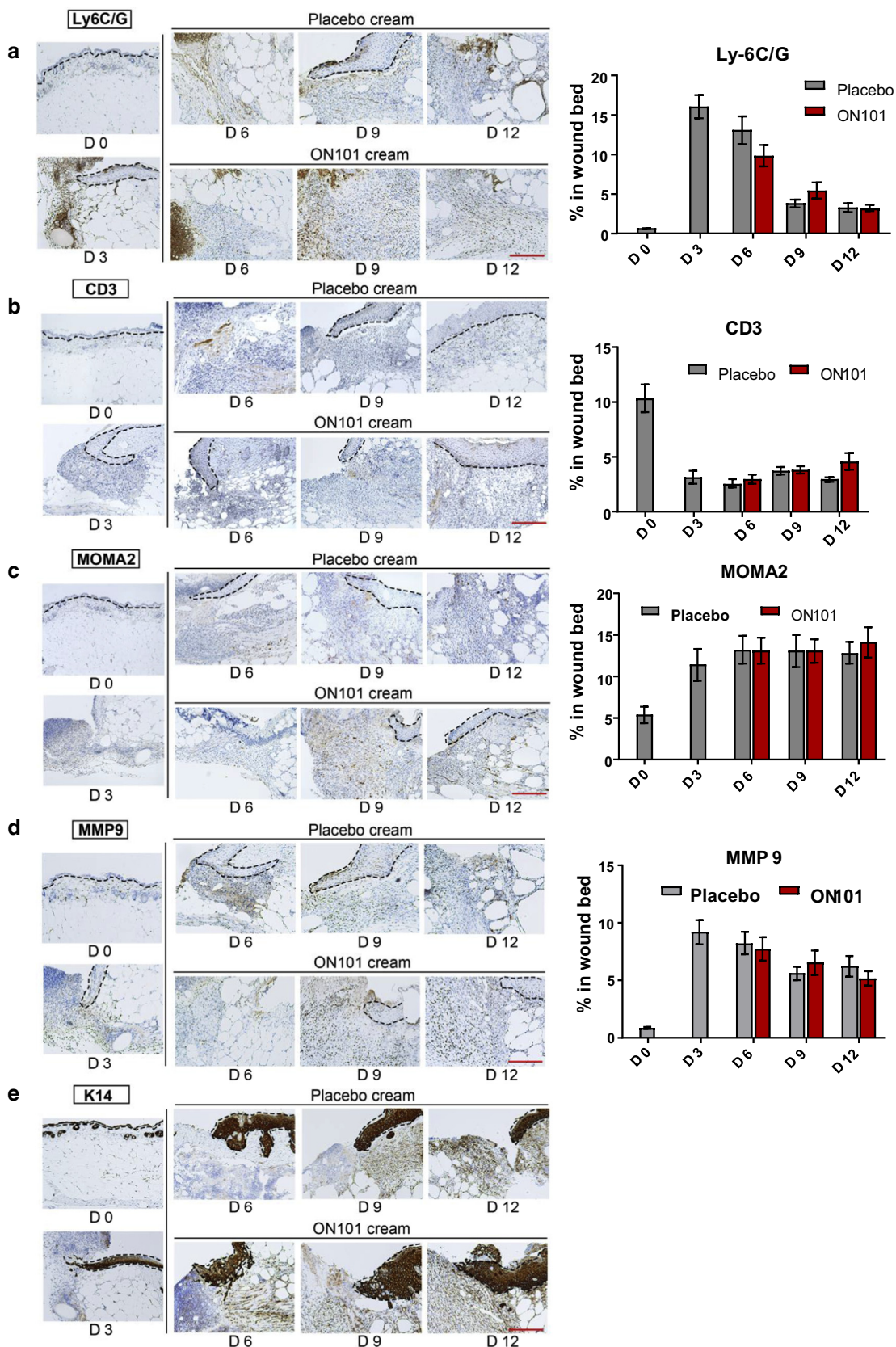


Figure 2. IHC staining and quantification of serial sections of biopsies from ON101- or placebo-treated wounds. (a–e) Images of IHC results for (a) anti-Ly-6C/6G, (b) anti-CD3, (c) anti-MOMA2, (d) anti-MMP9, and (e) anti-K14 within wound biopsies of db/db mice at the indicated time points. Quantified results for each antibody are shown on the right (except for anti-K14) and are expressed as means \pm SEMs ($n = 8$ per group). Bar = 250 μ m. D, day; IHC, immunohistochemistry; K14, keratin 14; MMP9, matrix metalloproteinase 9.

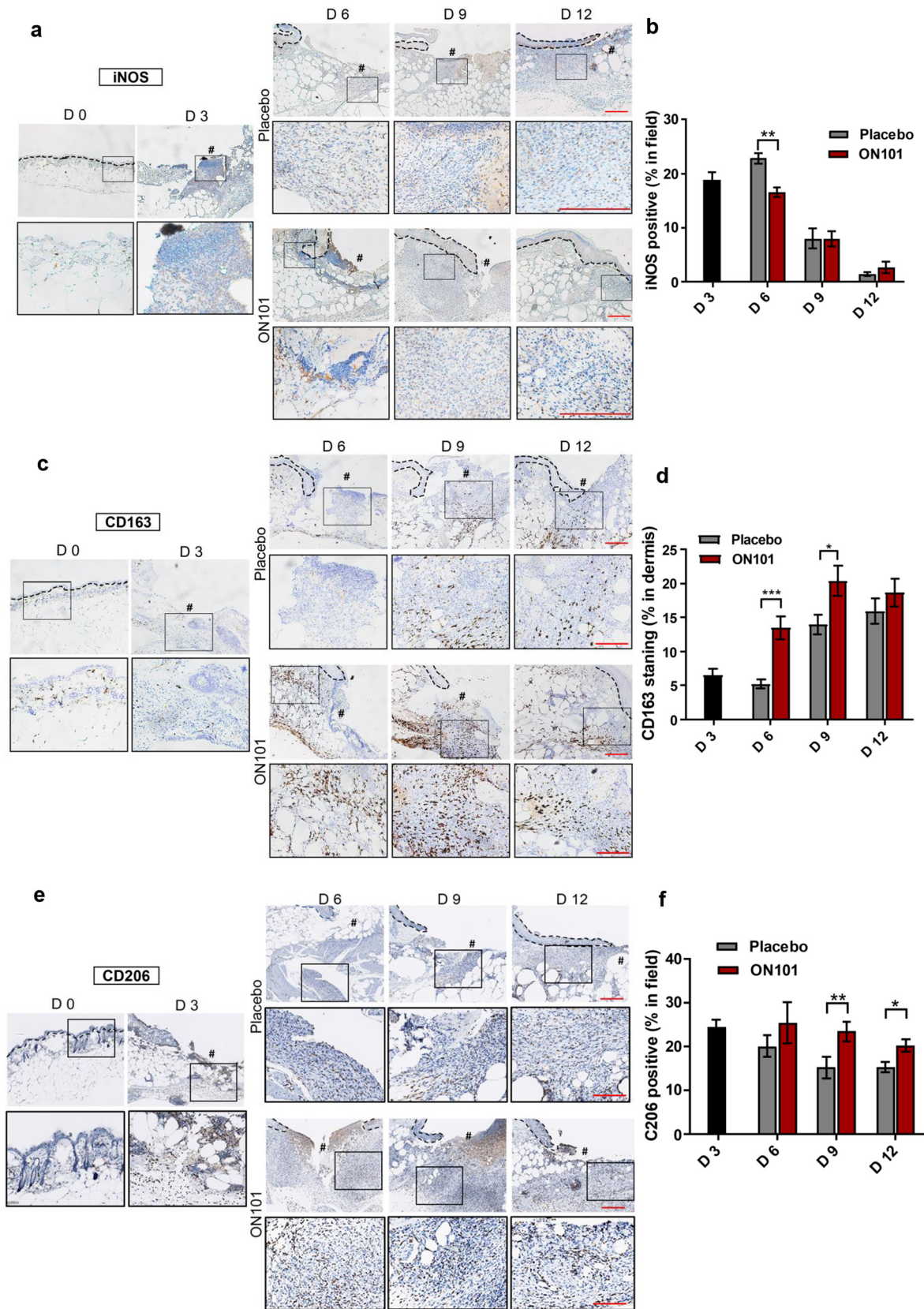


Figure 3. ON101 alters the population of iNOS⁺, CD163⁺, and CD206⁺ cells in diabetic wound surroundings. Immunohistochemical staining of wound biopsies from db/db mice for detecting (a) iNOS, (c) CD163, and (e) CD206. (b) Quantification of iNOS-positive stain in the whole field compared with that in the total tissue area; n = 8 selected fields per group. (d) Quantification of the CD163-positive stain in the dermis compared with total nuclear stain. n = 16 selected fields per group. (e) Quantification of the CD206-positive stain in the wound edge compared with the nuclear stain in the field. n = 8 selected fields per group. All values represent means ± SEM. Statistical analysis is based on the Student's *t*-test. **P* < 0.05, ***P* < 0.01, and ****P* < 0.001.

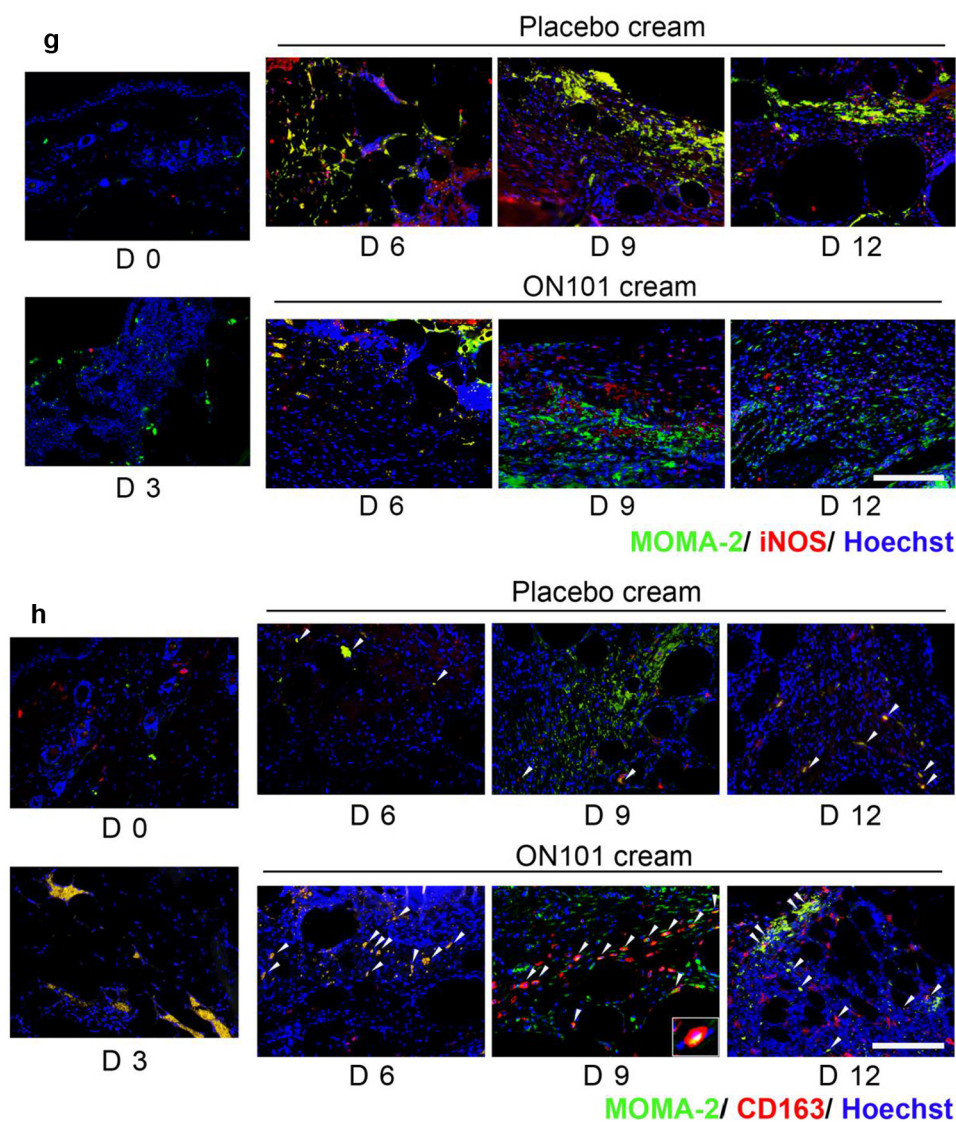


Figure 3. Continued. (g, h) Dual immunostaining of macrophage-related markers revealed partial localization of iNOS and CD163 with monocyte/macrophage marker. Immunofluorescence staining of sections of biopsies from ON101- or placebo-treated wounds at indicated time points. Bar = 250 μm. (g) MOMA2 (in green) and iNOS (in red) dual staining combined with Hoechst nuclear staining revealed that iNOS colocalized with macrophages in the placebo-treated control group, whereas iNOS was decreased and did not colocalize with MOMA2 in the ON101-treated group. (h) MOMA2 (in green) and CD163 (in red) dual staining combined with Hoechst nuclear staining revealed increased colocalization in ON101-treated groups compared with that in the placebo-treated controls. Arrow indicates colocalization. Bar = 150 μm. iNOS, inducible nitric oxide synthase.

members caused by prolonged maintenance of M1 macrophages within the wound area impedes M2 macrophage polarization and damages surrounding tissues (Seraphim et al., 2020).

Considerable effort has been devoted to understanding the pathology of diabetic foot ulcers and identifying the possible strategies for resolving ulcer chronicity and avoiding severe consequences such as amputation (Frykberg and Banks, 2015). Accordingly, approaches designed to rebalance the M1/M2 ratio by reducing the proportion of M1 macrophages or minimizing pro-inflammatory cues possess therapeutic potential for promoting diabetic wound healing (Hu et al., 2020; Nguyen et al., 2020; Perrault et al., 2018). In line with this treatment rationale, bioengineered materials designed to enhance M2 macrophage infiltration or topically administered exosomes derived from M2 macrophages have been applied in patients (Gan et al., 2019; Ishida et al., 2019; Kim et al., 2019). Both approaches showed that enrichment of M2 macrophages and reversing imbalanced M1/M2 ratios accelerated diabetic wound healing.

ON101, a topical cream formulated using identified, defined fractions of *Plectranthus amboinicus* (PA-F4) and *Centella asiatica* (S1) in a proprietary ratio, has been reported to be capable of inhibiting NLRP3 inflammasome signaling and regulating macrophages (Huang et al., 2021; Leu et al., 2019). Having established the clinical efficacy of ON101 in promoting wound healing in randomized controlled studies (Huang et al., 2021; Leu et al., 2019), in this study, we further explore the details of the molecular mechanism by which ON101 regulates cell function and cellular networks to improve healing in diabetic wounds and gain insight into the macrophage phenotypes involved in diabetic foot ulcers.

RESULTS

ON101 promotes wound healing in two animal models of diabetic wound healing

We first confirmed ON101's healing activity in two mouse models of type 2 diabetes: high-fat diet (HFD)-induced diabetes and genetically obese db/db mice. The wound recovery rate was slower in diabetic wounds than in normal wounds in both mouse models (Figure 1a and b for HFD and Figure 1c

and d for db/db). For the HFD model, obesity-induced hyperglycemia and insulin resistance were established by feeding an HFD for 10 weeks. After wounding, mice from both diabetic models received either a placebo or ON101 cream topically. The wound recovery rate was significantly faster in the ON101-treated group than in the placebo group from day 6 to day 9 in the HFD mouse model (Figure 1a and b). Consistent with this, ON101 significantly promoted diabetic wound healing in db/db mice compared with placebo from day 6 to day 12 after treatment (Huang et al., 2021) (Figure 1c and d). Histological examinations showed that more granulation tissue appeared on day 6, and faster epithelization was observed on day 9 in the ON101-treated group than in the placebo group (Figure 1e). Together, these results indicate that ON101 effectively accelerates wound healing in a diabetic milieu compared with placebo controls regardless of the pathological process by which diabetes is generated.

ON101 treatment alters the populations of macrophage subtypes and modulates gene expression profiles in diabetic wounds

Perturbed inflammatory cues are a major cause of impaired diabetic wound healing (Eming et al., 2014; MacLeod and Mansbridge, 2016). We first performed immunohistochemistry (IHC) to determine whether ON101 affected specific types of immune cells, including neutrophils (anti-Ly6G/6C), T cells (anti-CD3), and monocytes/macrophages (anti-MOMA2) (Figure 2a–c). The fibroblast marker matrix metalloproteinase 9 (Liu et al., 2009) and epithelial marker keratin 14 were also analyzed (Figure 2d and e). Quantifications revealed that neutrophils, fibroblasts, and T cells appeared in the first 3 days after wounding, and the expression of each marker decreased gradually during the healing process without a significant difference between ON101 and placebo groups (Figure 2a and b and d). On the other hand, total monocyte and macrophage counts increased from day 0 to day 6, with no significant differences in overall cell numbers stabilizing from day 6 to 12 (Figure 2c) between the two groups.

Among monocytes and macrophages, the inducible nitric oxide synthase (iNOS)-positive M1 subtype of macrophages decreased over time (Figure 3a and b and g). Specifically, the proportion of iNOS⁺ cells was reduced significantly around wound edges in the ON101-treated group on day 6 after wounding compared with that in the placebo group (Figure 3b). The increased number of CD163⁺ cells was observed on day 6 (Figure 3c and d and h), whereas the expression pattern of CD206⁺ cells was marked enriched after wounding on day 3 (Figure 3e and f), indicating earlier CD206⁺ enrichment than CD163⁺. In addition, the proportions of CD163⁺ and CD206⁺ cells were increased from day 6 in ON101-treated wounds compared with that in placebo groups (Figure 3d and f). The iNOS-MOMA2 or CD163-MOMA2 double-staining images showed that a decreased number of iNOS⁺MOMA⁺ double-positive staining in the ON101-treated group (Figure 3g) and a greater number of CD163⁺MOMA2⁺ could be observed in the ON101-treated group than in their corresponding placebo controls (Figure 3h). These results imply that ON101 treatment might

modulate the proportion of M1 and M2 macrophages around the diabetic wound bed.

To quantify the dynamic changes in macrophage subtypes induced by ON101, macrophages isolated from wound-surrounding tissues of db/db mice treated with either ON101 or placebo cream were analyzed by flow cytometry (Figure 4a). These analyses confirmed a gradual increase of total macrophages (F4/80⁺) around the wound but without significant differences between groups (Figure 4b). Notably, the proportion of CD163⁺ cells among all macrophages (CD163⁺ in F4/80⁺ cells) was significantly increased in the ON101-treated group compared with that in the placebo group (Figure 4c), indicating enhanced recruitment or increased numbers of M2c-like macrophages in the ON101-treated group. In addition, a lower non-M2 cells/M2 ratio was observed in the ON101-treated group on days 6 and 9 compared with that in the placebo group (Figure 4e), suggesting that ON101 may modulate the population of macrophage subtypes.

Next, we explored which genes might be affected by ON101 in diabetic wounds. A total of 86 wound healing-related genes were analyzed using a TaqMan Array Mouse Wound Healing Panel (Supplementary Table S1). Confirmed by qRT-PCR, several M1-associated genes, including *Ifn γ* , *Il1 α* , *Cxcl1*, and *Cxcl11*, were downregulated, whereas the M2-associated gene *Il4* was upregulated by ON101 treatment (Figure 4e and f). In addition, genes likely involved in lymphocyte recruitment and differentiation, such as *Cxcl3* and *Gcsf* (Martin et al., 2021; Reyes et al., 2021), were also upregulated by ON101 treatment (Figure 4f). These results suggest that topical application of ON101 downregulates proinflammation-associated genes and upregulates M2-associated genes and other genes related to chemoattraction or cell differentiation in a diabetic wound.

ON101 directly suppresses M1 macrophage polarizing and restores CD206⁺ M2 macrophages by reversing M1-mediated M2 suppression

Poor glycemic control in patients with diabetes is often associated with chronic inflammation and elevated levels of proinflammatory cytokines (Chang and Yang, 2016). To test the M1 or M2 polarization under our conditions, the polarizable human monocyte cell line, THP-1, was used to polarize M1 or M2 macrophages under either normal-glucose or high-glucose (HG) conditions. The results show that the proportion of CD86 and CD80 (M1 markers) was higher among cells cultured in HG than in those cultured in normal-glucose conditions (Figure 5a and b). In contrast, the proportion of M2a/c markers (CD163⁺ and/or CD206⁺) after M2-polarizing conditions was lower in the HG medium than in the normal-glucose medium (Figure 5c and d).

After establishing this model and under the same experimental conditions, increasing concentrations of ON101 were cultured with the cells in the M1-polarizing condition, which led to a dose-dependent suppression in the proportion of CD86- and CD80-positive M1 macrophages (Figure 5e). This was not attributable to nonspecific cytotoxic effects (Figure 5g). *Cd80* and *Cd86* mRNA levels were also downregulated by ON101 (Figure 5f), suggesting that ON101 transcriptionally suppressed CD80 and CD86. In contrast, in

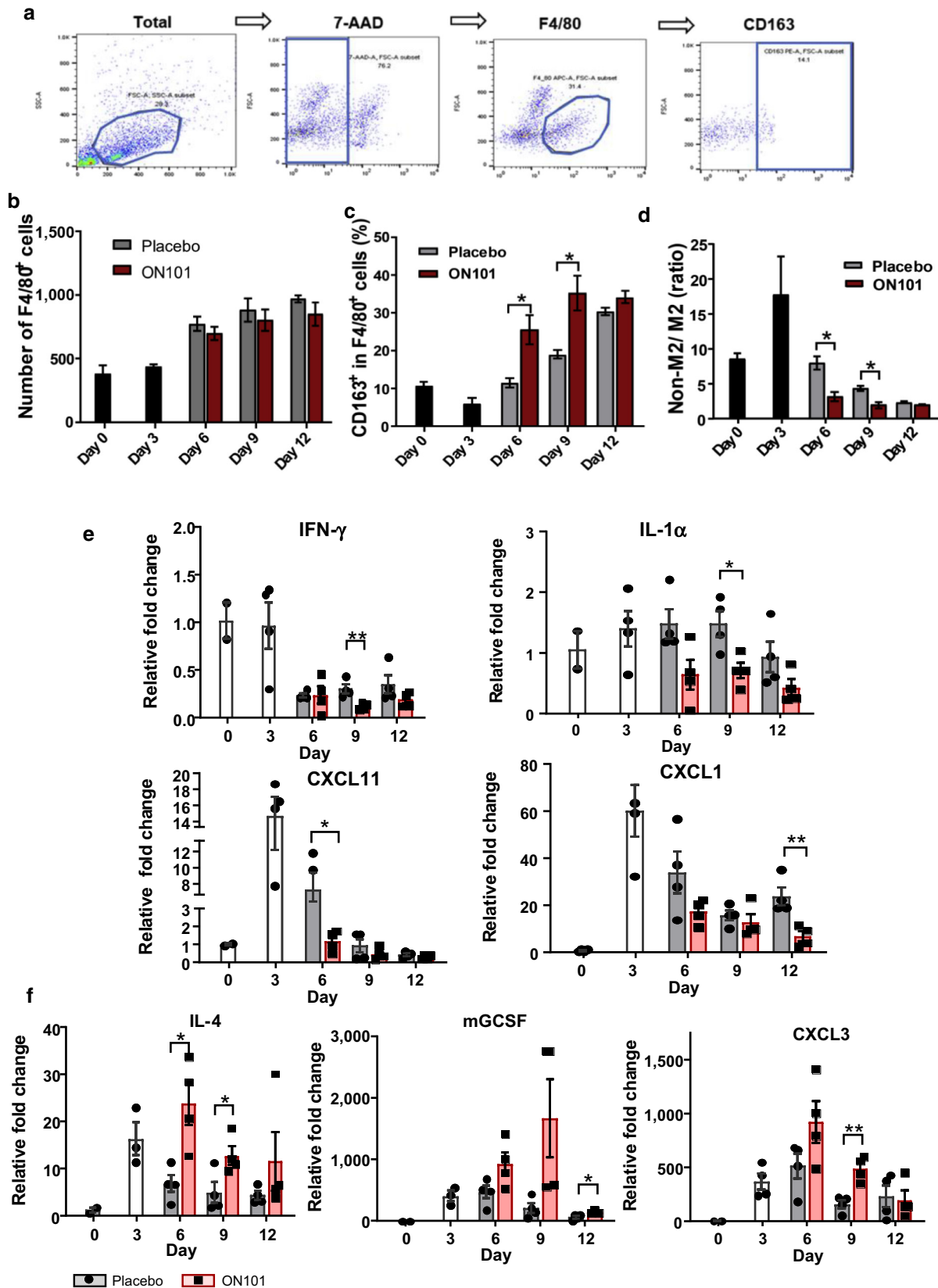


Figure 4. ON101 alters the dynamics of macrophage subtypes and the transcriptional expression profile of inflammation-associated cytokines in db/db mice. (a) Gating strategy for analyzing the macrophage subtypes in a diabetic wound. (b–d) FACS analysis of macrophage subtypes in diabetic wounds. $n = 3$ mice per group. (b) The number of F4/80-positive macrophages around wound beds in db/db mice after treatment with ON101 or placebo cream. A fixed number of cells (5×10^4) was gated, and the F4/80-positive population was quantified after excluding dead cells using 7-AAD viability staining. (c) Quantification of the percentage of CD163⁺ cells among F4/80⁺ cells in each wound. (d) The ratio of cell numbers in the non-M2 population/M2⁺ population in each wound sample. (e, f) Relative expressions (normalized with GAPDH and compared with that on day 0) of (e) proinflammatory cytokine genes and (f) macrophage-associated

the in vitro M2 macrophage polarization model, ON101 did not affect the expression levels of CD163 or CD206, suggesting that ON101 does not directly affect M2 polarization (Figure 5h).

Ex vivo M1 polarization experiments isolated from human PBMCs further revealed that although basal amounts of CD14⁺/CD68⁺/CD86⁺ and CD14⁺/CD68⁺/CD80⁺ cells differed among six donors, the proportions of CD86⁺ and CD80⁺ levels appeared to be suppressed in a concentration-dependent manner by coadministering ON101 in HG medium (Figure 5i). Collectively, these findings show that ON101 directly inhibits M1 polarization by suppressing the expressions of CD80 and CD86.

To further explore whether ON101 alters M1 macrophage functions, we performed RNA sequencing (Figure 6a). A total of 121 genes changed after ON101 treatment (Supplementary Table S2). qRT-PCR validation showed that ON101 downregulated the M1-associated chemokines *CXCL9*, *CXCL10*, and *CCL12*, which function in T helper 1-mediated immune activation (Kuo et al., 2018) (Figure 6b). *CCL2* and *CCL3*, cytokines involved in monocyte and/or macrophage recruitment and migration (Schraufstatter et al., 2012; Zhuang et al., 2019), were significantly upregulated by ON101 treatment (Figure 6b). In addition, an examination of proinflammatory cytokines released from ex vivo-polarized M1 macrophages from six independent donors revealed that ON101 significantly suppressed the levels of IL-6, IL-1 β , and TNF- α (Figure 6c). These findings show that ON101 treatment alleviates M1-associated inflammation and provides an environment that favors monocyte recruitment.

To determine whether M1-dominated proinflammatory cues impair the polarization of M2 macrophages, we collected conditioned medium (CM) from M1 polarization cultures (M1-associated CM [M1-CM]) and cotreated with M2-polarizing agents to see the extent of M2 polarization as shown in Figure 7a. Flow cytometry analyses showed that M1-CM dramatically suppressed the expression of both CD206 and CD163 during the M2-polarization process (Figure 7b). By contrast, ON101-treated M1-CM significantly rescued the levels of CD206-positive macrophages but not those of CD163 (Figure 7b). In addition, M1-CM increased CD80 and CD86 levels in M2 macrophages, whereas ON101-treated M1-CM downregulated both CD86 and CD80 expression (Figure 7c). These results reveal the repressive role of factors secreted from M1 macrophages to counter a microenvironment favoring M2 polarization. Thus, ON101 is likely to function in mitigating the M1-dominant milieu, changing it to an M2a-favorable environment.

ON101 enhances the activity of adipocyte progenitor cells to promote M1-to-M2 transition

Adipocyte progenitor cells (ADPCs), identified by their positive staining for Pref-1, are skin-resident mesenchymal stem cells with multiple regenerative potentials that mediate skin regeneration and diabetic wound repair (Gadelkarim et al.,

2018; Sul, 2009). There was a noticeable increase in Pref-1-positive cells around the subcutaneous fat layer during the wound healing process in ON101-treated db/db mice compared with that in mice in the placebo group (Figure 8a), suggesting that ON101 might activate ADPCs.

Because ON101 treatment increased the expression of CD163⁺ cells during the healing process in mice with diabetes, we further evaluated whether ON101 promoted CD163⁺ M2 polarization through the activation of adipocyte stem cells. To test this, CM from cultures of ADPCs (ADPC-associated CM), with or without ON101 treatment, was applied to the M1 polarization assay (Figure 8b). ADPC-associated CM significantly suppressed CD80 and CD86 (Figure 8c) but only slightly increased the intensity of CD163 and CD206 (Figure 8d). Interestingly, the application of ON101-treated ADPC-associated CM significantly increased the intensities of both CD206 and CD163 markers (Figure 8d), suggesting that ADPCs play a significant role in ON101-induced promotion of the M1-to-M2 transition.

ON101 stimulates ADPC expression of GCSF and CXCL3, which are engaged in the M1-to-M2 transition

We next analyzed whether the genes altered by ON101 treatment in diabetic wounds could be produced by ADPCs during ON101 treatment and focused on candidate genes detected in wound tissues in ON101-treated db/db mice (Figure 4e and f). The qRT-PCR results showed that ON101 induced a concentration-dependent increased expression of *GCSF* and *CXCL3* (Figure 8e) but not that of other genes in ADPCs (Figure 8f). To test whether *GCSF* and *CXCL3* might be involved in the marker switch between M1 and M2 macrophages, recombinant *GCSF* and *CXCL3* proteins, with or without their neutralizing antibodies, were coadministered with M1-polarizing cytokines. *GCSF* treatment caused a concentration-dependent increase in both CD163 and CD206 (Figure 8g), whereas *CXCL3* treatment only induced CD163 expression (Figure 8h). Both *GCSF*- and *CXCL3*-mediated inductions of M2a/c markers were abolished by the corresponding neutralizing antibodies (Figure 8g and h). In addition, both *GCSF* and *CXCL3* treatments activated signal transducer and activator of transcription 3 (STAT3) signaling pathways, whereas *GCSF* activated protein kinase B phosphorylation, which was again abolished by their corresponding antibodies (Figure 8i). These results reveal that ON101 can readily stimulate both *GCSF* and *CXCL3* gene expression in ADPCs and that their expressions may subsequently promote the activation of CD206⁺ and/or CD163⁺ M2 subtypes in M1 macrophages.

M2 macrophages are critical for ON101-accelerated wound healing

Because ON101 exerts dual effects on M1/M2 ratios, downregulating M1 and promoting M2 macrophages, we first clarified whether M2 macrophages are critical for normal wound healing by a loss-of-function assay of M2 macrophages. Mannosylated clodronate (m-Cl_o) was applied to deplete M2 macrophages (Chu et al., 2019). Mice were

cytokine genes in ON101- or placebo cream-treated wounds in db/db mice, determined by qRT-PCR (n = 4 mice per group). Gene expression levels were normalized to those of endogenous *GAPDH*. Data are shown as means \pm SEM. Student's *t*-test. **P* < 0.05, ***P* < 0.01, and ****P* < 0.001. 7-AAD, 7-aminoactinomycin D; FSC-A, forward scatter area; K, thousand; SSC-A, side scatter area.

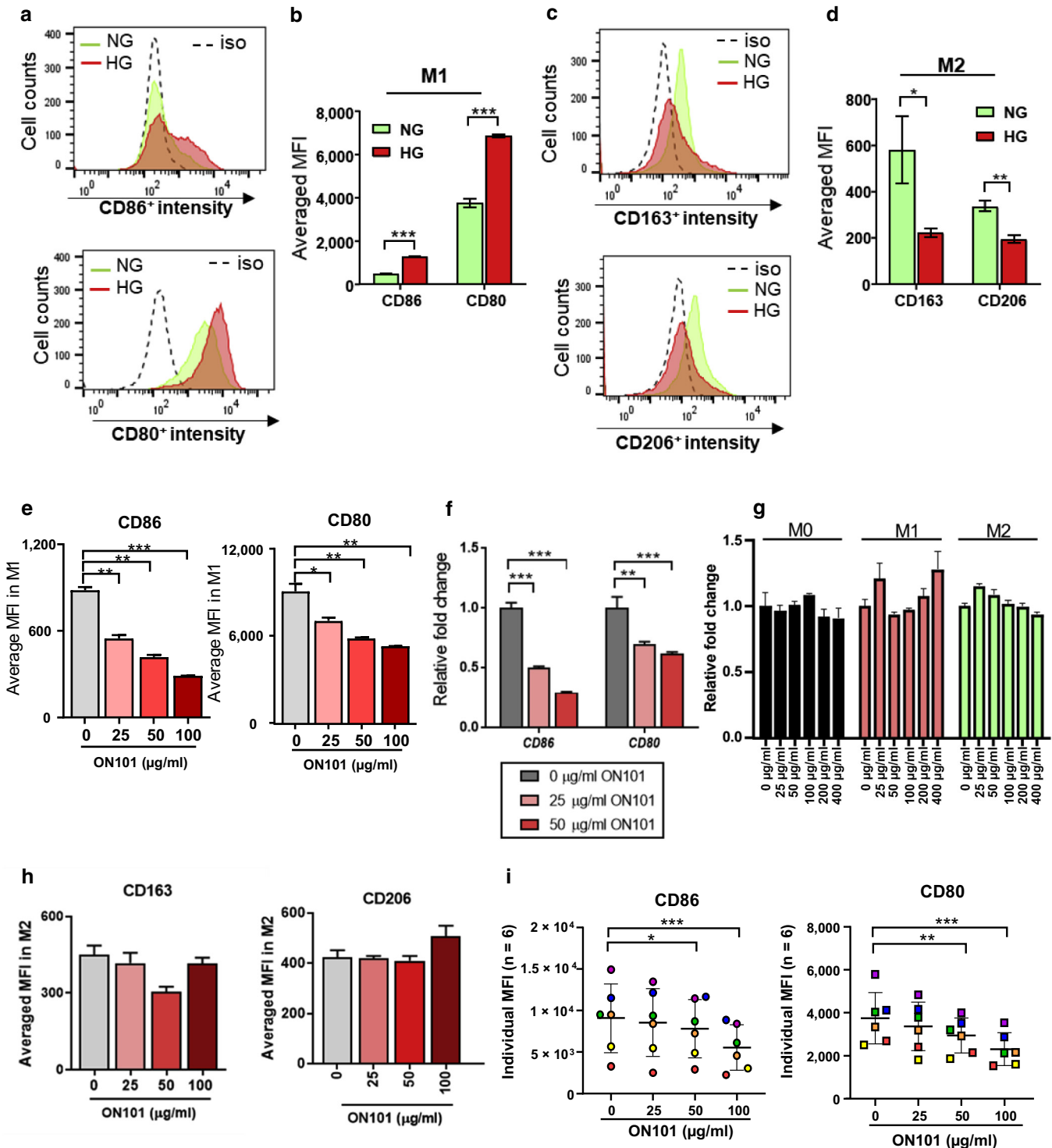


Figure 5. ON101 directly attenuates M1 markers under HG conditions. THP-1-derived (a, b) M1 and (c, d) M2 polarization models in culture medium containing NG (1,000 mg/l glucose) or HG (4,500 mg/l glucose), as determined by flow cytometry. (a) Representative histograms showing CD86 and CD80 intensity cultured under M1-polarizing conditions in NG or HG medium. (b) Summary data calculated from three independent experiments showing the MFIs for CD86 and CD80. (c) Representative histograms show CD163 and CD206 expression intensities under M2-polarizing conditions in NG or HG medium. (d) Summary data calculated from three independent experiments showing MFIs for CD163 and CD206. Data are shown as means \pm SEM. Statistical analysis is based on the Student's *t*-test. * $P < 0.05$, ** $P < 0.01$, and *** $P < 0.001$. (e) MFI values and (f) fold changes in the gene expressions of *CD86* and *CD80* induced by ON101 in M1 macrophages (compared with 0 $\mu\text{g/ml}$ of ON101). (g) Cell viability assays of THP-1-derived M0, M1, and M2 macrophages after ON101 treatment for 48 h. The results were standardized against the control group for each cell type. (h) MFIs of CD163 and CD206 after a 48-h treatment with an M2-polarizing cocktail and different concentrations of ON101 as indicated. Data are shown as means \pm SEMs of three independent experiments. (i) M1 macrophages derived from human PBMCs treated with ON101 for 96 h. Markers were analyzed by FACS ($n = 6$; paired Student's *t*-test). Data are shown as means \pm SEM; Student's *t*-test. ** $P < 0.01$ and *** $P < 0.001$. h, hour; HG, high glucose; iso, isotype control; MFI, mean fluorescence intensity; NG, normal glucose.

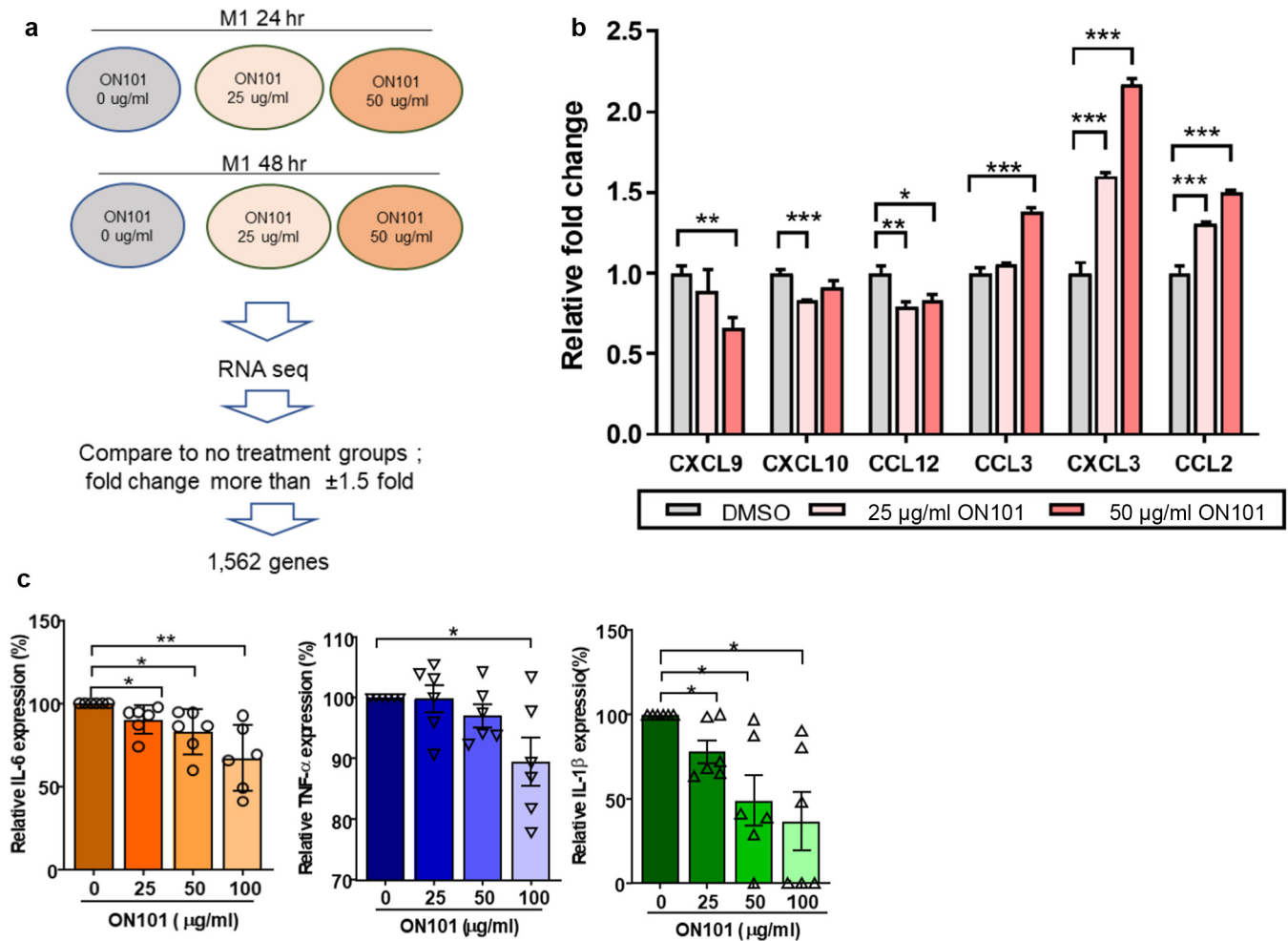


Figure 6. ON101 modulates M1-associated cytokine release and gene expressions under high-glucose conditions. (a) Experimental design and data analysis flow chart to reveal the gene expression profiles in M1 macrophages after ON101 treatment evaluated by RNA sequencing. (b) Cytokine/chemokine gene expressions altered by 48 hrs of ON101 treatments in M1 macrophages analyzed by q-RT-PCR. DMSO serves as a control treatment. Data are shown as means \pm SEMs of three independent experiments. (c) Relative levels of secreted proinflammatory cytokines measured by ELISA for 24 hrs (IL-6 and TNF- α) and 96 hrs (IL-1 β) after M1-polarizing (n = 6 individual donors; paired Student's *t*-test). Data are shown as means \pm SEM. ***P* < 0.01 and ****P* < 0.001. hr, hour; RNA seq, RNA sequencing..

pretreated with m-Clo or control liposomes (m-Encapsomes) for 7 days before wounding and then continued being treated for 6 days after wounding (Figure 9a). CD163⁺ M2 macrophages were efficiently depleted by m-Clo as determined by flow cytometry (Figure 9c). Compared with wound healing in the m-Encapsomes-treated group, wound healing was delayed in the m-Clo-treated group, suggestive of the vital role of M2 macrophages in normal wound healing (Figure 9b).

Further testing sought to evaluate whether ON101 treatment can promote diabetic wound healing by enriching the population of M2 macrophages. After the administration of m-Clo or m-Encapsomes, db/db mice were cotreated with ON101 or placebo cream after wounding (Figure 9d). ON101 treatment improved the wound healing rate compared with the placebo treatment; notably, this effect was abolished by reducing the proportion of M2 macrophages through m-Clo treatment (Figure 9e and f). Flow cytometry analysis of M2 macrophages further indicated that ON101-accelerated wound healing was accompanied by an

increase in the population of CD163⁺ macrophages, an effect that was also effectively attenuated by m-Clo treatment (Figure 9g). IHC staining showed a thin dermis layer and a deficiency of CD163⁺ and CD206⁺ cells around the wound bed in the m-Clo-treated group (Figure 9h). In addition, the extracellular matrix remodeling protein, α -smooth muscle actin as well as Pref-1⁺ cells were markedly increased in the ON101-treated group, effects that were attenuated by M2 depletion (Figure 9h). On the basis of these results, we conclude that topical ON101 treatment promotes diabetic wound healing through dual pathways—attenuated M1-mediated proinflammatory cues and enhanced M2 macrophage populations—by enabling the M1-to-M2 transition through factors secreted by ADPCs. Thus, ON101 facilitates diabetic wound healing through an M2-macrophage-dependent pathway.

DISCUSSION

Dysregulation of macrophage subsets manifests as a defect in the M1-to-M2 transition and is recognized as the primary

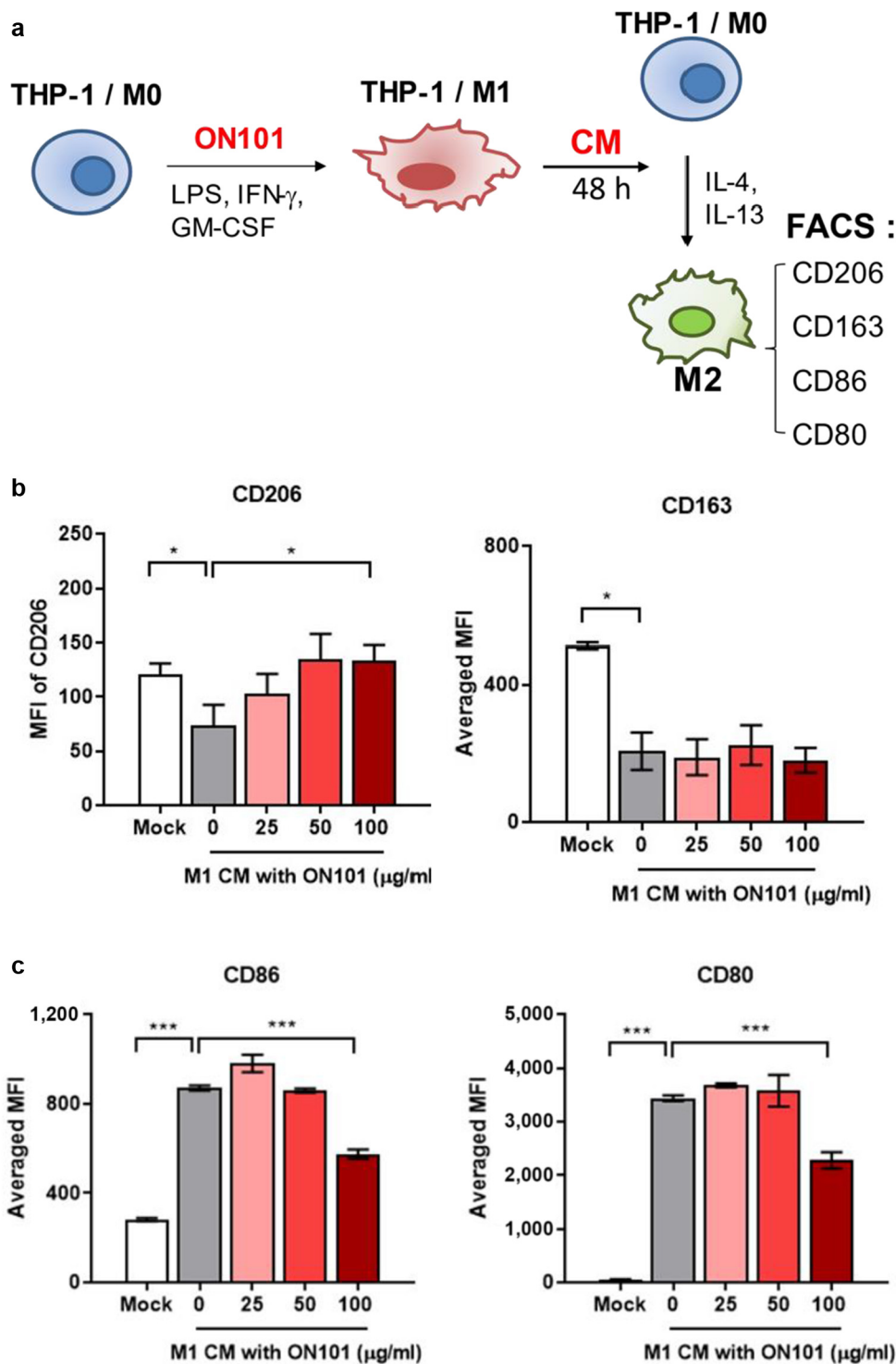


Figure 7. ON101 attenuates M1-mediated M2a marker expression. (a) Schematic depicting the experimental flowchart. MFI values for (b) CD163⁺ and CD206⁺ M2 macrophage populations and (c) CD80⁺ and CD86⁺ M1 macrophage markers under M2-polarization conditions were analyzed by flow cytometry 48 h after M2 polarization. Data are shown as means \pm SEM of three experiments. Statistical analysis is based on the Student's *t*-test. ***P* < 0.01 and ****P* < 0.001. CM, conditioned medium; h, hour; MFI, mean fluorescence intensity.

factor that impedes diabetic wound healing (Boniakowski et al., 2017; Khanna et al., 2010). Research-based on reshaping the M1/M2 populations has failed to yield an effective solution (Ganesh and Ramkumar, 2020; Raziyeve et al., 2021). We identified ON101 as a drug that efficiently accelerates diabetic wound healing dually through attenuating M1 macrophage polarization and activating ADPCs, thereby creating an environment favoring the M1-to-M2 transition. ON101 simultaneously promotes this

transition through multiple cellular pathways involving macrophages and ADPCs, altering their chemokine/cytokine profiles to promote polarization toward both prohealing M2a and proremodeling M2c macrophages. Such a mechanism has successfully improved diabetic wound healing clinically (Huang et al., 2021). These findings show proof of concept with respect to how medicinal plant ingredients can reshape macrophage subtypes that are critical in the coordinated process of healing complicated dermal wounds.

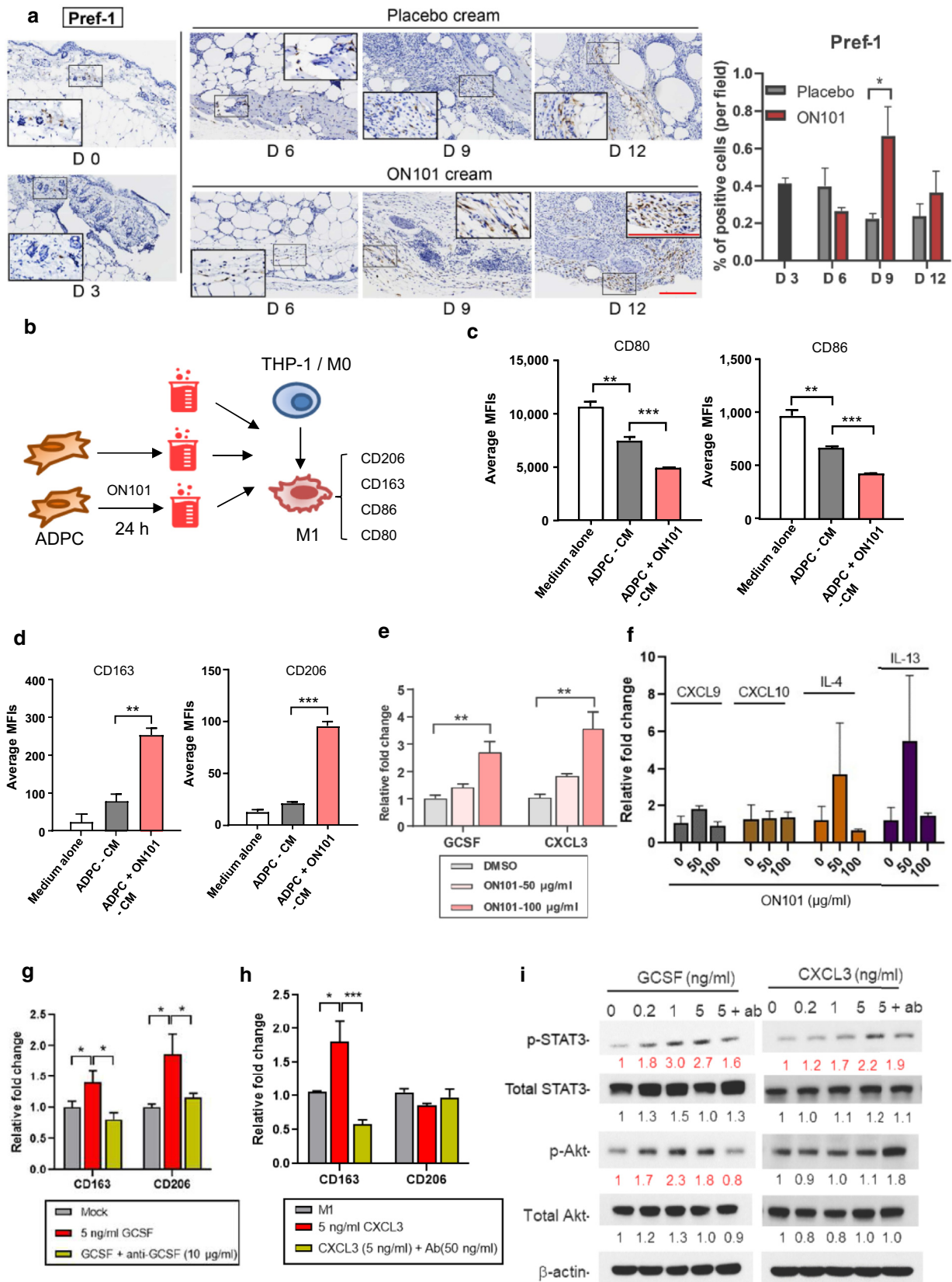


Figure 8. ON101 promotes M1-to-M2 macrophage transition through ADPC-mediated production/secretion of GCSF and CXCL3. (a) Immunohistochemical detection of Pref-1 in wound biopsies from db/db mice and quantified results using an area quantification module with 16 selected fields per group. Bar = 100 µm. (b–d) Schematic of CM collected from ADPCs treated with ON101 for 24 h for the second round of M1 polarization. MFIs for (c) M1 markers and (d) M2 markers detected by FACS 48 h after M1 polarization. Expression of (e) *GCSF* and *CXCL3* genes or other (f) indicated cytokines in human ADPCs after 24 h of ON101 treatment, determined by qRT-PCR. (g, h) Expression of CD163 and CD206 after coadministration of recombinant (g) GCSF or (h) CXCL3 protein and (i) Western blot analysis of p-STAT3, Total STAT3, p-Akt, Total Akt, and beta-actin in human ADPCs after 24 h of ON101 treatment.

The proinflammatory cytokines, IL-1 β and TNF- α , secreted primarily from M1 macrophages perpetuate inflammation in the diabetic wound (Mouritzen et al., 2021; Razyieva et al., 2021). Topical application of anti-IL-1 β - or anti-TNF- α -neutralizing antibodies promotes the recruitment of healing-associated CD206⁺ macrophages around the wound and accelerates wound healing (Goren et al., 2007; Mirza et al., 2013). Thus, a reduction in wound inflammation favors the presence of M2-like macrophages and also improves wound healing. Our results showed that ON101 attenuated the production of the M1-associated cytokines and that CM from ON101-treated M1 macrophages prevented the expression of M1 markers, showing that ON101 suppresses M1-mediated chronic inflammation around the wound and thus creates an environment favorable for M2 recruitment and polarization.

Although the M2a and M2c subtypes are considered pro-healing (CD206-dominant) and proremodeling (CD163-dominant) macrophages, respectively, the detailed functions of distinct M2 subsets and regulation of their plasticity in the skin have not yet been fully elucidated (Nakai, 2021). We found that CXCL3 has the ability to activate CD163, whereas GCSF is capable of enhancing the expression of both CD206 and CD163 markers representative of the M2a/c subtypes. These findings show that in addition to the standard in vitro M2a priming cytokines IL-4/IL-13 and M2c priming cytokine IL-10 (Graney et al., 2020), GCSF and CXCL3 may play roles in regulating the plasticity of M2a and M2c during certain circumstances of wound healing.

GCSF is a hematopoietic differentiation factor predominantly secreted by bone marrow-derived progenitor cells that promotes granulocyte differentiation through STAT3- or phosphoinositide-3 kinase-mediated axes (Lachmann et al., 2015). We found that both phosphorylated STAT3 and phosphorylated protein kinase B levels were increased in response to GCSF treatment and abolished by GCSF-neutralizing antibodies, correlating with corresponding trends in the regulation of M2 markers. Interestingly, a systematic study that analyzed the major M1-to-M2 macrophage-polarizing pathways showed that activation of STAT3 signaling in M2 macrophages was predominantly driven by IL-10 (Zhao et al., 2021). Collectively, this study and others suggest that STAT3 pathway activation by GCSF or IL-10 is crucial for promoting M2 macrophage polarization.

Autologous fat or ADPC grafts are currently considered treatment approaches currently for chronic wound healing (Nolan et al., 2021). In addition, the secretomes derived from ADPCs can attenuate pathogenic inflammation by promoting both the recruitment and polarization of M2 macrophages (Kruger et al., 2018; Zhao et al., 2018). However, the factors secreted by ADPCs that influence M2 macrophages have not been fully identified (Kruger et al., 2018; Zhao et al., 2018). We showed in this study that CM from ON101-treated

ADPCs induced the expression of CD206 and CD163, suggesting that ON101 might indirectly promote the generation of M2a/M2c macrophages by modulating the secretion of GCSF and CXCL3 from ADPCs. However, whether there are other factors secreted from ON101-challenged ADPCs needs to be further investigated. ON101 treatment may therefore be a more effective and convenient therapeutic for activating ADPCs in situ rather than transplanting live ADPCs into wounds, which may be expensive and require considerable time to perform.

In summary, we found that ON101, a medicinal plant agent, exhibits a unique function in accelerating diabetic wound healing by attenuating chronic inflammation through the suppression of M1-macrophage polarization and activity. Then, ON101 generates a milieu favorable for the enrichment of M2 macrophages by stimulating the secretion of CXCL3 and GCSF from ADPCs. Our findings showed that ON101-mediated reorchestrating of the distribution of immune cells and their messengers increases diabetic wound healing abilities and may therefore be another therapeutic option for treating complicated diabetic foot ulcers.

MATERIALS AND METHODS

Drug formulation

ON101 cream and placebo cream were used in animal experiments. ON101 cream contains 1.25% of ON101 powder and was manufactured as previously described (Huang et al., 2021). Placebo cream is the cream-based vehicle control containing no ON101. For in vitro assays, ON101 powder was dissolved in DMSO (D12345, Thermo Fisher Scientific, Waltham, MA) at a stock concentration of 25 mg/ml.

Animal models of diabetes

All animal experiments were approved by the Institutional Animal Care and Use Committee of Oneness Biotech (Taipei, Taiwan). Mice were housed in standard conditions of 25 °C with a 12/12-hour light–dark cycle with ad libitum access to food and water. Male leptin receptor-deficient (db/db) mice aged 9 weeks (C57BLKS/J lar-+ Lepr^{db}/+Lepr^{db}, Institute for Animal Reproduction, Ibaraki, Japan) with fasting blood glucose levels of 300–500 mg/dl and body weight >35 g were assigned randomly to groups for drug treatments. Two full-thickness wounds were created on the back of each mouse using a sterile 6-mm biopsy punch. The wounds were covered with silicone splints (inner/outer diameter of 10/14 mm) to anchor them and reduce skin contraction and then covered with a transparent occlusive dressing (Tegaderm, 3M, Saint Paul, MN). ON101 (1.25%) or a placebo cream were applied topically once daily from day 3 after wounding to the date the mice were sacrificed.

For HFD mouse model experiments, male C57BL/6 mice aged 6 weeks (BioLASCO, Taipei, Taiwan) were fed an HFD for rodents containing 60 kcal of fat for 10 weeks. An oral glucose tolerance test was used to evaluate whether an HFD-induced obesity model had been established, defined as a mean 60-minute oral glucose

← corresponding antibodies with M1-polarizing cytokines for 48 h. Data are shown as means \pm SEM of three experiments. (i) Immunoblots of p-STAT3, total STAT3, p-Akt, and total Akt during treatments. β -actin was used as a protein loading control. Concentrations: 1 μ g/ml for anti-GCSF and 50 ng/ml for anti-CXCL3. All statistical data was conducted by Student's *t*-test. **P* < 0.05, ***P* < 0.01, and ****P* < 0.001. Ab, antibody; ADPC, adipocyte progenitor cell; Akt, protein kinase B; CM, conditioned medium; h, hour; m-Clo, m-Clo, mannosylated Clodosome; m-Enc, m-Encapsome; MFI, mean fluorescence intensity; p-Akt, phosphorylated protein kinase B; p-STAT3, phosphorylated signal transducer and activator of transcription 3; STAT3, signal transducer and activator of transcription 3.

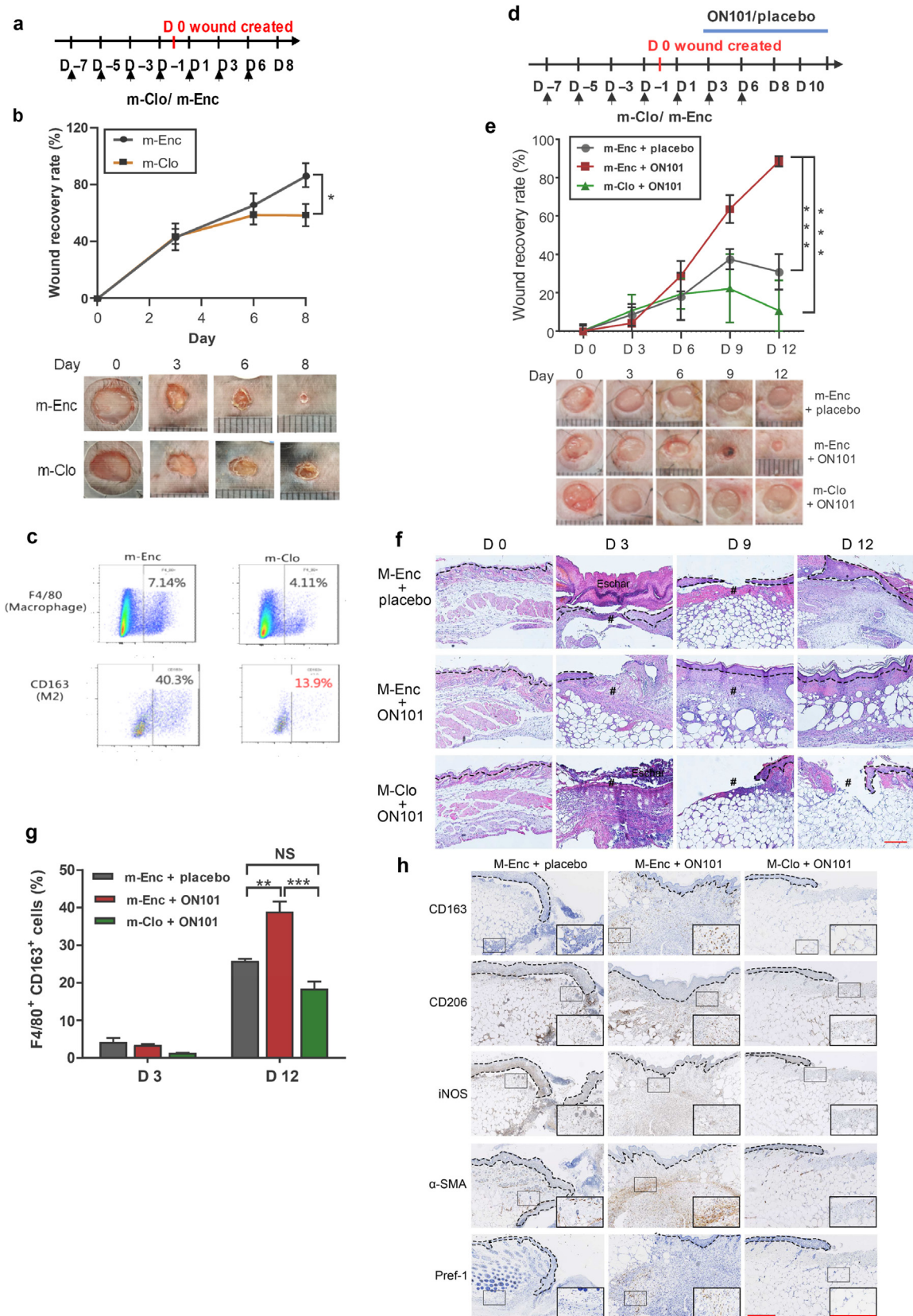


Figure 9. M2 macrophages are required for normal as well as ON101-enhanced diabetic wound healing. (a–c) Subcutaneous injection of m-Clo or m-Enc during normal wound healing in C57BL/6 mice. (a) Schematic; n = 4 mice per group. (b) Wound recovery rate, calculated as the percentage change from the original size (day 0) and images of wounds at the indicated times. (c) Biopsies from the point of wounding were analyzed by flow cytometry to detect the proportions of M2 macrophages (F4/80⁺/CD163⁺) at indicated time point. Data represent the percentages of F4/80⁺ or CD163⁺ macrophages. (d–h) M2 macrophage dependence of ON101-promoted diabetic wound healing. m-Clo/m-Enc. (d) Schematic; n = 4 mice per group. (e) Wound recovery rate

Table 1. Antibody List

Reactive Species	Application	Antibody List (Information)
mouse	IHC	Against CD163 (ab182422, Abcam, Cambridge, United Kingdom), iNOS (E-AB-70051, Elabscience, Houston, TX), CD206 (ab64693, Abcam), cytokeratin 14 (ab181595, Abcam), Ly6G/6C (ab2557, Abcam), MMP9 (ab228402, Abcam), CD3 (ab16669, Abcam), MOMA2 (ab33451, Abcam), and α SMA (ab32575, Abcam).
mouse	Flow	APC-conjugated anti-mouse F4/80 (17-4801-82, eBioscience, San Diego, CA) and PE-conjugated anti-mouse CD163 (12-1631-82, eBioscience) and 7-AAD (A1310, Thermo Fisher Scientific, Waltham, MA)
human	Western blot	p-STAT3 antibody (number 9131S), STAT3 antibody (number 9139S), p-Akt antibody (number 9271), and Akt antibody (number 9272S), Cell Signaling Technology, Danvers, MA). Proteins were detected by enhanced chemiluminescence.
human	Flow cytometry	PE CF594-conjugated anti-hCD68 (BD Biosciences, Franklin Lakes, NJ), FITC-conjugated anti-hCD86 (BioLegend, San Diego, CA), PE/Dazzle 594-conjugated anti-hCD80 (BioLegend), Pacific Blue-conjugated anti-hCCR7 (BioLegend), PE-conjugated anti-hCD163 (BioLegend), BV605-conjugated anti-hCD206 (740417, BD Bioscience), and BV510-conjugated anti-FVS (564406, BD Biosciences).

Abbreviations: α SMA, α -smooth muscle actin; 7-AAD, 7-aminoactinomycin D; APC, allophycocyanin; Akt, protein kinase B; IHC, immunohistochemistry; iNOS, inducible nitric oxide synthase; MMP9, matrix metalloproteinase 9; p-Akt, phosphorylated protein kinase B; PE, phycoerythrin; p-STAT3, phosphorylated signal transducer and activator of transcription 3; STAT3, signal transducer and activator of transcription 3.

tolerance test value in the HFD group that was significantly higher than that in the normal diet control group (mean blood glucose level at 60 minutes after oral glucose tolerance test = 385 mg/dl). After the HFD-induced obesity model was established, mice were randomly divided into placebo- or ON101-treated groups and wounded as described earlier.

For M2 macrophage depletion experiments, C57BL/6N mice aged 8 weeks (BioLASCO) or db/db mice were fed standard chow and water. Mice were allocated randomly to receive either mannosylated Clodrosome (mannosylated liposomes that contain clodronate) or control m-Encapsome (Encapsula NanoSciences, Brentwood, TN) subcutaneously at a dose of 0.05 mg/kg every 2 days from 7 days before wounding until the end of the experiment. ON101-containing or placebo creams were applied topically daily from day 3 after wounding.

Images of wounds were acquired at the indicated time points, and wound areas in images were calculated using ImageJ software (National Institutes of Health, Bethesda, MD).

Table 2. Primer List

Gene Name	Primer Sequence(5'–3')
<i>mIFNγ</i>	F: CGGCACAGTCATTGAAAGCCTA R: GTTGCTGATGGCCTGATTGTC
<i>mIL1a</i>	F: ACGGCTGAGTTTCAGTGAGACCTT R: AGGTGTAAGGTGCTGATCTGGGTT
<i>mCXCL1</i>	F: GCTTGAAGGTGTTGCCCTCAG R: AAGCCTCGCGACCATTCTTG
<i>mCXCL11</i>	F: AGGAAGGTACAGCCATAGC R: CGATCTCTGCCATTTTGACG
<i>mIL4</i>	F: AGATGGATGTGCCAAACGTCCTCA R: AATATGCGAAGCACCTTGGAAAGCC
<i>mCSF3</i>	F: TGGCAGCAGATGGAAAACCTAG R: AGGTACGAAATGGCCAGGACA
<i>mCXCL3</i>	F: AGATCTCACCACAGCCCTTC R: AACCTTGGTAGGGTGTCA
<i>mGAPDH</i>	F: CGACTTCAACAGCAACTCCCCTCTTCC R: TGGGTGGTCCAGGGTTTCTTACTCCTT
<i>hCD80</i>	F: CTCACTTCTGTTCCAGGTGTATCCA R: TCCTTTTGCCAGTAGATGCCA
<i>hCD83</i>	F: TCCTGAGCTGCGCCTACAG R: GCAGGGCAAGTCCACACTCTT
<i>hCD86</i>	F: CTGTAACCTCCAGCTGTCTCCGTA R: GCCCATAAGTGTGCTCTGAAGTGA
<i>hCXCL9</i>	F: CCAACACCCACAGAAGTGC R: GCCAGCACCTGCTCTGAGAC
<i>hCXCL10</i>	F: GAACTGTACGCTGTACTCGGA R: TTGATGGCTTCGATTCTGGA
<i>hCCL12</i>	F: TCAGCTGAGCTACAGATGC R: CTTTAGCTTCGGGTCAATGC
<i>hCCL3</i>	F: TCAGACTTCAGAAGGACACGG R: CTGCATGATTCTGAGCAGGTG
<i>hCXCL3</i>	F: AAGTGTGAATGTAAGGTCCCC R: GTGCTCCCCTTGTTCAGTATC
<i>hCCL2</i>	F: AGGTGACTGGGGCATTGAT R: GCCTCCAGCATGAAAGTCTC
<i>hCSF3</i>	F: GCTGCTTGAGCCAACTCCATA R: GAACGCGGTACGACACCTC
<i>hGAPDH</i>	F: ACATCGCTCAGACACCATG R: TGTAGTTGAGGTCAATGAAGGG

Abbreviations: F, forward; h, human; m, murine; R, reverse.

IHC staining and quantification

Full-thickness biopsy samples of skin tissue around wound edges were fixed in 10% paraformaldehyde followed by embedding in paraffin wax and sectioned at 5 μ m intervals. IHC was performed (with a routine antigen-retrieval procedure) using antibodies as listed in Table 1. Whole-tissue scans were analyzed with HALO software (Indica Labs, Albuquerque, NM) using Area Quantification, version 1.0; Cytonuclear, version 1.5; and Cytonuclear FL, version 1.4, modules.

The quantification procedure of all IHC slides was performed using HALO software (Indica Labs) after whole slide scanning was performed using Aperio AT2 (Leica, Wetzlar, Germany). The wound

(percentage change from day 0) and images of wounds at the indicated times for each treatment group. (f) H&E staining represents re-epithelization (dotted line) and the WB in the indicated treatment. (g) FACS analysis of the proportions of M2 macrophages (F4/80⁺/CD163⁺) in wound surroundings. (h) IHC staining of wound biopsies with indicated antibodies on day 9 after wounding. # denotes wound bed. Bar = 250 μ m. Data represent means \pm SEM. *P* values in **b** and **e** were analyzed using two-way repeated-measures ANOVA, whereas that in **g** was analyzed using Student's *t*-test. **P* < 0.05, ***P* < 0.01, and ****P* < 0.001. α -SMA, α -smooth muscle actin; m-Enc, m-Encapsome; IHC, immunohistochemistry; iNOS, inducible nitrate oxide synthase; NS, not significant. m-Clod, mannosylated Clodrosome; WB, wound bed.

Table 3. Baseline Value for Isotype Controls

Antibody	Isotype	Mean	Median
CD80	PE/CF594	180	87.8
CD86	FITC	324	168
CD163	PE	120	96.4
CD206	BV605	90.4	69.0

Abbreviation: PE, phycoerythrin.

bed and surrounding tissue were first circled for quantification. For antigens that belong to membrane staining, such as CD163, CD206, CD3, and MOMA2, the multiplex module was used to calculate the relative percentage of positive cells. For antibodies against cytoplasm proteins such as iNOS, matrix metalloproteinase 9, and Ly-6C/6G, an area quantification module was used to calculate the area of positive tissue/total area of the tissue of interest, expressed as a percentage. All of the quantifications were normalized with hematoxylin stain.

qRT-PCR

Skin tissue was first homogenized using a TissueLyser LT (Qiagen, Hilden, Germany) with homogenization beads. Total RNA from in vitro cultured cells and skin tissues was extracted at different time points using GENEzol TriRNA Pure kits (Geneaid Biotech, New Taipei City, Taiwan) and reverse transcribed into cDNA using First Strand cDNA Synthesis kits (Thermo Fisher Scientific). qRT-PCR analyses were performed on a QuantStudio 6 Flex Real-Time PCR System using SYBR Green qRT-PCR Master Mix (both from Thermo Fisher Scientific). Primer sequences used for these experiments are listed in Table 2.

Detection of mouse skin immune cells by flow cytometry

Collected skin samples were first incubated in 0.25% Trypsin-EDTA for 30 minutes and subsequently 2 mg/ml collagenase at 37 °C for 1.5 hours. After wash, cells were filtered by 70 and 40- μ m strainers and conjugated with antibodies as listed in Table 1 in staining buffer for 30 minutes. FACS analyses of stained cells were performed using a FACSaria Fusion Flow Cytometer (BD Biosciences, Franklin Lakes, NJ). All flow cytometry data were analyzed by FlowJo 6.0 software (BD Biosciences.)

Cell culture and M1 and M2 polarization

THP-1 cells were first polarized to M0 status by treatment with 60 ng/ml phorbol myristate acetate (Sigma-Aldrich, St. Louis, MO) for 24 hours and rested for an additional 24 hours. For M1 polarization, cells were induced by incubating with 20 ng/ml IFN- γ (R&D Systems, Minneapolis, MN), 1 μ g/ml lipopolysaccharide (Sigma-Aldrich), and 20 ng/ml GM-CSF (R&D Systems) for 48 hours. For M2 polarization, M0 cells were treated with IL-4 and IL-10 (20 ng/ml; both from R&D Systems) for 48 hours. For polarization procedures, cells were cultured in either an HG medium containing 4,500 mg/l glucose or a normal-glucose medium containing 1,000 mg/l glucose as indicated in Figure legends.

Human ADPCs were obtained from GICC Medical (New Taipei City, Taiwan). For gene expression analyses, ADPCs were seeded at a density of 6×10^4 cells/ml in 12-well plates and incubated overnight. The next day, the cells were treated with 25, 50, or 100 ng/ml ON101 or vehicle control and incubated for 24 hours.

PBMCs separated from blood obtained from six healthy donors were processed for monocyte isolation as previously described (Zarif et al., 2016). CD14⁺ cells were polarized into M1 or M2

macrophages by incubating with 20 ng/ml GM-CSF (R&D Systems) and M-CSF (R&D Systems) for 4 days. Thereafter, M1 macrophages were generated by treatment with 20 ng/ml IFN- γ , 1 μ g/ml lipopolysaccharide, and 20 ng/ml GM-CSF. Different concentrations of ON101 were administered together with these cytokines for 48 hours during the M1 polarization process.

Detection of human macrophage markers by flow cytometry

For detection of M1 and M2 macrophage markers, cultured cells were suspended and then blocked by 20 μ l/10⁴ of FcR Blocking Reagent (Miltenyi Biotec, Cologne, Germany). Antibodies listed in Table 1 and isotype signals for normalization listed in Table 3 were used at 5 μ l per 10⁵ cells.

ELISAs

Culture media were collected from PBMC-derived M1 and M2 macrophages at the indicated time points. ELISA kits for TNF- α (number DY210), IL-6 (number DY206), and IL-1 β (number DY201) were purchased from R&D Systems, and the experiments were performed according to the manufacturer's instructions. Plates were analyzed by measuring the light absorbance of wells at 450 nm using a microplate reader (Synergy H1 Hybrid Reader, BioTek, Winooski, VT).

Cell lysate preparation and immunoblotting

Cell lysates for immunoblotting were prepared using an M-PER mammalian protein extraction kit containing protease and phosphatase inhibitor cocktail (Thermo Fisher Scientific). Immunoblotting using the indicated antibodies (listed in Table 1) was performed as described previously (Lu et al., 2020).

Statistical analysis

All statistical comparisons were performed using GraphPad Prism 7 (GraphPad Software, San Diego, CA). Unpaired two-tailed Student's *t*-tests were used to compare datasets between two independent groups and paired Student's *t*-tests were used for comparing means within the same group. The difference between the two groups was conducted by two-way ANOVA with Tukey's posthoc test for multiple pairwise comparisons. Data are presented as means \pm SEM, and differences with a *P* < 0.05 were considered statistically significant.

Data availability statement

No datasets were generated or analyzed during this study.

ORCIDiS

Ching-Wen Lin: <http://orcid.org/0000-0001-8984-1137>

Chih-Chiang Chen : <http://orcid.org/0000-0002-5723-6730>

Wen-Yen Huang : <http://orcid.org/0000-0001-9625-0802>

Yen-Yu Chen : <http://orcid.org/0000-0002-6716-3985>

Shiou-Ting Chen : <http://orcid.org/0000-0003-3010-3652>

Hung-Wen Chou: <http://orcid.org/0000-0003-3568-7845>

Chien-Ming Hung : <http://orcid.org/0000-0002-9218-7065>

Wan-Jiun Chen : <http://orcid.org/0000-0003-2239-3127>

Chia-Sing Lu: <http://orcid.org/0000-0001-5941-3406>

Shi-Xin Nian: <http://orcid.org/0000-0003-3423-5759>

Shyi-Gen Chen: <http://orcid.org/0000-0001-6796-8188>

Hsuen-Wen Chang: <http://orcid.org/0000-0002-0464-9822>

Vincent H.S. Chang: <http://orcid.org/0000-0001-9056-152X>

Li-Ying Liu: <http://orcid.org/0000-0001-8560-3035>

Ming-Liang Kuo: <http://orcid.org/0000-0001-8634-3696>

Shun-Cheng Chang: <http://orcid.org/0000-0002-3335-7298>

AUTHOR CONTRIBUTIONS

Conceptualization: CWL, CCC, VHSC, MLK; Formal Analysis: CMH; Investigation: WYH, YYC, STC, HWC, SXN, CSL, SWC, LYL; Project Administration: CWL, WJC; Supervision: MLK, SCC, SGC; Writing – Original Draft Preparation: CWL; Writing - Review and Editing: WYH, MLK, SCC.

ACKNOWLEDGMENT

We acknowledge the support of Peggy Tseng (BOI HUI Biotech) for the characterization of the purity of adipocyte-derived stem cells. Adipocyte-derived stem cells and human PBMCs were conveyed through institutional review board number B202005048, Tri-Service General Hospital (Taipei, Taiwan). We thank DerMEDit (www.dermedit.com) for language editing services that were paid for by Oneness Biotech. This work was funded by Oneness Biotech.

CONFLICT OF INTEREST

CWL, YYC, HWC, WJC, and SGC are employers in Oneness Biotech. WYH, STC, and CMH are employers in Microbio. MLK is an employer in Microbio Shanghai. The remaining authors state no conflict of interest.

SUPPLEMENTARY MATERIAL

Supplementary material is linked to the online version of the paper at www.jidonline.org, and at <https://doi.org/10.1016/j.xjidi.2022.100138>

REFERENCES

- Abdelaziz MH, Abdelwahab SF, Wan J, Cai W, Huixuan W, Jianjun C, et al. Alternatively activated macrophages; a double-edged sword in allergic asthma. *J Transl Med* 2020;18:58.
- Boniakowski AE, Kimball AS, Jacobs BN, Kunkel SL, Gallagher KA. Macrophage-mediated inflammation in normal and diabetic wound healing. *J Immunol* 2017;199:17–24.
- Chang SC, Yang WV. Hyperglycemia, tumorigenesis, and chronic inflammation. *Crit Rev Oncol Hematol* 2016;108:146–53.
- Chu SY, Chou CH, Huang HD, Yen MH, Hong HC, Chao PH, et al. Mechanical stretch induces hair regeneration through the alternative activation of macrophages. *Nat Commun* 2019;10:1524.
- Eming SA, Martin P, Tomic-Canic M. Wound repair and regeneration: mechanisms, signaling, and translation. *Sci Transl Med* 2014;6:265sr6.
- Frykberg RG, Banks J. Challenges in the treatment of chronic wounds. *Adv Wound Care (New Rochelle)* 2015;4:560–82.
- Gadelkarim M, Abushouk AI, Ghanem E, Hamaad AM, Saad AM, Abdel-Daim MM. Adipose-derived stem cells: effectiveness and advances in delivery in diabetic wound healing. *Biomed Pharmacother* 2018;107:625–33.
- Gan J, Liu C, Li H, Wang S, Wang Z, Kang Z, et al. Accelerated wound healing in diabetes by reprogramming the macrophages with particle-induced clustering of the mannose receptors. *Biomaterials* 2019;219:119340.
- Ganesh GV, Ramkumar KM. Macrophage mediation in normal and diabetic wound healing responses. *Inflamm Res* 2020;69:347–63.
- Gordon S. Alternative activation of macrophages. *Nat Rev Immunol* 2003;3:23–35.
- Goren I, Müller E, Schiefelbein D, Christen U, Pfeilschifter J, Mühl H, et al. Systemic anti-TNF α treatment restores diabetes-impaired skin repair in ob/ob mice by inactivation of macrophages. *J Invest Dermatol* 2007;127:2259–67.
- Graney PL, Ben-Shaul S, Landau S, Bajpai A, Singh B, Eager J, et al. Macrophages of diverse phenotypes drive vascularization of engineered tissues. *Sci Adv* 2020;6:eaay6391.
- Hu J, Zhang L, Liechty C, Zgheib C, Hodges MM, Liechty KW, et al. Long noncoding RNA GAS5 regulates macrophage polarization and diabetic wound healing. *J Invest Dermatol* 2020;140:1629–38.
- Huang SM, Wu CS, Chiu MH, Wu CH, Chang YT, Chen GS, et al. High glucose environment induces M1 macrophage polarization that impairs keratinocyte migration via TNF- α : an important mechanism to delay the diabetic wound healing. *J Dermatol Sci* 2019;96:159–67.
- Huang YY, Lin CW, Cheng NC, Cazzell SM, Chen HH, Huang KF, et al. Effect of a novel macrophage-regulating drug on wound healing in patients with diabetic foot ulcers: A randomized clinical trial. *JAMA Netw Open* 2021;4:e2122607.
- Ishida Y, Kuninaka Y, Nosaka M, Furuta M, Kimura A, Taruya A, et al. CCL2-mediated reversal of impaired skin wound healing in diabetic mice by normalization of neovascularization and collagen accumulation. *J Invest Dermatol* 2019;139:2517–27.e5.
- Khanna S, Biswas S, Shang Y, Collard E, Azad A, Kauh C, et al. Macrophage dysfunction impairs resolution of inflammation in the wounds of diabetic mice. *PLoS One* 2010;5:e9539.
- Kim H, Wang SY, Kwak G, Yang Y, Kwon IC, Kim SH. Exosome-guided phenotypic switch of M1 to M2 macrophages for cutaneous wound healing. *Adv Sci (Weinh)* 2019;6:1900513.
- Kruger MJ, Conradie MM, Conradie M, van de Vyver M. ADSC-conditioned media elicit an ex vivo anti-inflammatory macrophage response. *J Mol Endocrinol* 2018;61:173–84.
- Krzyszczak P, Schloss R, Palmer A, Berthiaume F. The role of macrophages in acute and chronic wound healing and interventions to promote pro-wound healing phenotypes. *Front Physiol* 2018;9:419.
- Kuo PT, Zeng Z, Salim N, Mattarollo S, Wells JW, Leggatt GR. The role of CXCR3 and its chemokine ligands in skin disease and cancer. *Front Med (Lausanne)* 2018;5:271.
- Lachmann N, Ackermann M, Frenzel E, Liebhaber S, Brenning S, Happle C, et al. Large-scale hematopoietic differentiation of human induced pluripotent stem cells provides granulocytes or macrophages for cell replacement therapies. *Stem Cell Rep* 2015;4:282–96.
- Leu WJ, Chen JC, Guh JH. Extract From *Plectranthus amboinicus* Inhibit Maturation and Release of interleukin 1beta Through Inhibition of NF-kB Nuclear Translocation and NLRP3 inflammasome Activation. *Front Pharmacol* 2019;10:573.
- Liu Y, Min D, Bolton T, Nubé V, Twigg SM, Yue DK, et al. Increased matrix metalloproteinase-9 predicts poor wound healing in diabetic foot ulcers: response to Muller et al. *Diabetes Care* 2009;32:e137.
- Lu CS, Lin CW, Chang YH, Chen HY, Chung WC, Lai WY, et al. Antimetabolite pemetrexed primes a favorable tumor microenvironment for immune checkpoint blockade therapy. *J Immunother Cancer* 2020;8:e001392.
- MacLeod AS, Mansbridge JN. The innate immune system in acute and chronic wounds. *Adv Wound Care (New Rochelle)* 2016;5:65–78.
- Martin KR, Wong HL, Witko-Sarsat V, Wicks IP. G-CSF — a double edge sword in neutrophil mediated immunity. *Semin Immunol* 2021;54:101516.
- Mirza RE, Fang MM, Ennis WJ, Koh TJ. Blocking interleukin-1beta induces a healing-associated wound macrophage phenotype and improves healing in type 2 diabetes. *Diabetes* 2013;62:2579–87.
- Mouritzen MV, Petkovic M, Qvist K, Poulsen SS, Alarico S, Leal EC, et al. Improved diabetic wound healing by LFCinB is associated with relevant changes in the skin immune response and microbiota. *Mol Ther Methods Clin Dev* 2021;20:726–39.
- Nakai K. Multiple roles of macrophage in skin. *J Dermatol Sci* 2021;104:2–10.
- Nguyen VT, Farman N, Palacios-Ramirez R, Sbeih M, Behar-Cohen F, Aractingi S, et al. Cutaneous wound healing in diabetic mice is improved by topical mineralocorticoid receptor blockade. *J Invest Dermatol* 2020;140:223–34.e7.
- Nolan GS, Smith OJ, Jell G, Mosahebi A. Fat grafting and platelet-rich plasma in wound healing: a review of histology from animal studies. *Adipocyte* 2021;10:80–90.
- Perrault DP, Bramos A, Xu X, Shi S, Wong AK. Local administration of interleukin-1 receptor antagonist improves diabetic wound healing. *Ann Plast Surg* 2018;80:S317–21.
- Raziyeva K, Kim Y, Zharkinbekov Z, Kassymbek K, Jimi S, Saparov A. Immunology of acute and chronic wound healing. *Biomolecules* 2021;11:700.
- Reyes N, Figueroa S, Tiwari R, Geliebter J. CXCL3 signaling in the tumor microenvironment. *Adv Exp Med Biol* 2021;1302:15–24.
- Schraufstatter IU, Zhao M, Khaldoyanidi SK, Discipio RG. The chemokine CCL18 causes maturation of cultured monocytes to macrophages in the M2 spectrum. *Immunology* 2012;135:287–98.
- Seraphim PM, Leal EC, Moura J, Gonçalves P, Gonçalves JP, Carvalho E. Lack of lymphocytes impairs macrophage polarization and angiogenesis in diabetic wound healing. *Life Sci* 2020;254:117813.
- Sul HS. Minireview: Pref-1: role in adipogenesis and mesenchymal cell fate. *Mol Endocrinol* 2009;23:1717–25.
- Zarif JC, Hernandez JR, Verdones JE, Campbell SP, Drake CG, Pienta KJ. A phased strategy to differentiate human CD14+ monocytes into classically

- and alternatively activated macrophages and dendritic cells. *Bio-Techniques* 2016;61:33–41.
- Zhao C, Medeiros TX, Sové RJ, Annex BH, Popel AS. A data-driven computational model enables integrative and mechanistic characterization of dynamic macrophage polarization. *iScience* 2021;24:102112.
- Zhao H, Shang Q, Pan Z, Bai Y, Li Z, Zhang H, et al. Exosomes from adipose-derived stem cells attenuate adipose inflammation and obesity through polarizing M2 macrophages and beiging in white adipose tissue. *Diabetes* 2018;67:235–47.
- Zhuang Z, Yoshizawa-Smith S, Glowacki A, Maltos K, Pacheco C, Shehabeldin M, et al. Induction of M2 macrophages prevents bone loss in murine periodontitis models. *J Dent Res* 2019;98:200–8.



This work is licensed under a Creative Commons Attribution-NonCommercial-NoDerivatives 4.0 International License. To view a copy of this license, visit <http://creativecommons.org/licenses/by-nc-nd/4.0/>